Proceedings of International Conference on Heat Exchanger Fouling and Cleaning - 2011 (Peer-reviewed)
June 05 - 10, 2011, Crete Island, Greece
Editors: M.R. Malayeri, H. Müller-Steinhagen and A.P. Watkinson
Published online
www.heatexchanger-fouling.com

IMPACT OF THERMAL SHOCK ON FOULING OF VARIOUS STRUCTURED TUBES DURING POOL BOILING OF $CaSO_4$ SOLUTIONS

M. Evangelidou, M. Esawy and M.R. Malayeri

Institute for Thermodynamics and Thermal Engineering, University of Stuttgart, Pfaffenwaldring 6,
D-70550 Stuttgart, Germany, m.malayeri@itw.uni-stuttgart.de

ABSTRACT

Crystallization fouling during nucleate pool boiling is characterized with relatively rapid formation of a hard and brittle deposit layer. In this study, the impact of thermal shock is experimentally investigated on cleaning of various tubes when subjected to fouling of $CaSO_4$ solutions. The heat transfer tubes included stainless steel plain and finned tubes with fin densities of 19 and 40 fins per inch. The tubes were used during pool boiling for heat fluxes ranging from 80 to 300 kW/m². The thermal shock is applied by the sudden decrease or increase in heat flux for approximately 30 s after the fouling layer is formed. In terms of cleaning, the experimental results showed far better performance for the plain tube. During the sudden change in heat flux the whole fouling layer cracked and peeled off, receiving again almost initial clean heat transfer performance. Contrariwise, the results for the finned tubes showed that the fouling layer was only affected marginally by the thermal shock.

1. INTRODUCTION

The formation of crystal deposits on heat transfer surfaces is a common occurrence where aqueous solutions with inverse solubility are involved. The process is referred as crystallisation or precipitation fouling or simply scaling. The deposition of salts from solution is influenced by two processes of nucleation and crystal growth which can only occur when the solution is supersaturated at its respective temperature.

Crystallisation fouling is of concern for both forced convective and boiling modes of heat transfer but a much severe fouling is expected for the latter. This is because in boiling the surface temperature is well above the saturation temperature which results in generation of bubbles on the surface. Beneath the bubble, the concentration of foulant will increase due to steep temperature gradient. For salts with inverse solubility behaviour such as $CaSO_4$, concentration factors of 3-4 have been reported (Jamialahmadi and Müller-Steinhagen, 1993) resulting in rapid growth of deposit and the associated drop in heat transfer coefficient. This in turn gives rise to rapid formation of deposit beneath bubbles. Industries where crystallization fouling during boiling heat transfer is predominant include phosphoric acid plants (Behbahani et al., 2005), pulp mills (Gourdon et al., 2010), and steam generators (Schwarz, 2001).

Müller-Steinhagen et al. (2011) surveyed and categorized various techniques that are available to combat heat exchanger fouling. These techniques can be divided into two basic approaches of mitigation (including on-line cleaning) and off-line cleaning. It has however been reported that fouling may effectively be mitigated at the design stage of the heat exchanger. For instance, compact heat exchangers, such as plate and frame or spiral flow heat exchangers and fin-tube heat exchangers have been found to experience reduced fouling in many (but certainly not all) applications due to increased level of turbulence, reduced surface temperatures and homogenous flow distribution. While this has only been known for convective heat transfer to liquids, most recently Esawy et al. (2010) showed that the built-up of deposits during pool boiling of $CaSO_4$ solutions can substantially be reduced by the presence of fins on the tube outside.

Among other mitigation techniques, the impact of thermal shock maybe effective to clean the surface if the deposit is rigid and fragile. Difference in thermal expansion between the surface substrate and deposit layer plays a key role in this process. Nevertheless the experimental results on the impact of thermal shock are particularly scarce. In this study first the influence of surface geometry such as plain and finned structured tubes during pool boiling is examined. Fouling experiments have been performed using $CaSO_4$ as foulant. Thermal shock is then applied when the power to the heating elements is suddenly decreased or increased rapidly. For the plain tube, this has been repeated during an ongoing fouling run to discern the effectiveness of thermal shock. Finally, video recordings helped better insight into the bubble behaviour, built-up of deposit as time elapses and finally effectiveness of thermal shock when it was applied.

2. EXPERIMENTAL SET-UP AND PROCEDURE

A schematic diagram of the experimental setup is depicted in Fig 1. The test rig mainly consists of the boiling vessel (1) which is a cylindrical stainless steel tank with a capacity of 30 litres. The vessel is heated up by a resistance band heater. The connected flow loop, including the condenser (2) and electric resistance preheater (3), is

required for condensing and heating the evaporated liquid before re-entering it into the vessel respectively. The condenser is a co-current three stage single tube heat exchanger which can also be configured to a two or one stage heat exchanger. The cooling water mass flow is regulated by a manual flow control valve. The electrical rod heater (4) is mounted horizontally in the centre of the vessel and is fed by a power supply (max. 500 kW/m^2). The data acquisition system (5) connected to the computer (6) serves to record and analyse the measured data. For data acquisition, the Agilent 34970A with a 34910A armature multiplexer is used. Data is recorded on the computer via PCI-GPIB interface in a Microsoft Excel file. The front view port glass of the vessel allows video recording of the test run sequences. Videos (1000 fps) are recorded by the high speed camera Speed Cam Visario 1500 and saved via the software Visart 1.5 on the computer in AVI and JPEG format.

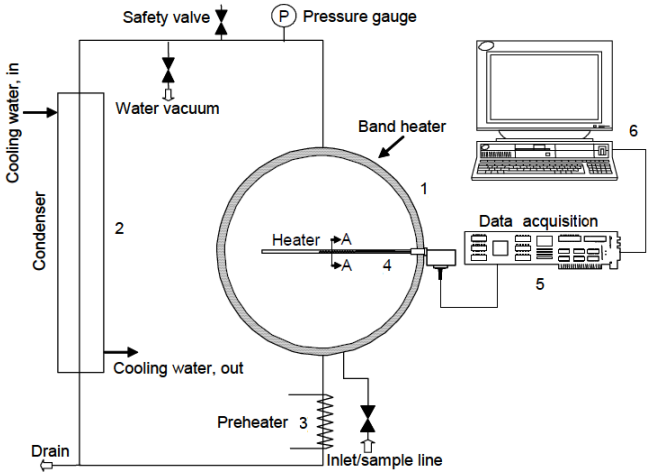

Fig 1 Schematic diagram of test rig.

2.1 Test tubes

The rod heater is manufactured by Ashland Chemical Company according to the specification of HTRI (Heat Transfer Research Incorporation). Four thermocouples (type E) are embedded inside the heater as shown in Fig. 2.

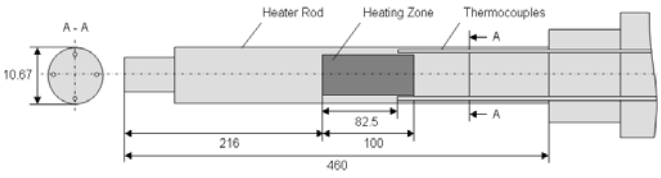

Fig. 2 HTRI rod heater (all dimensions in mm).

Three of these thermocouples are connected to the data acquisition system. The fourth one is used to regulate the power supply if the surface temperature exceeds a set limit. For minimizing the fluctuations of AC voltage, the power supply is connected to a voltage stabilizer. Two further thermocouples (type K) are located inside the vessel – one measures the bulk temperature and the other one is used to regulate the band heater of the vessel. For measuring the pressure inside the vessel an OMEGA PXM209 absolute pressure transducer is employed. In addition, the following data are measured and recorded by the data acquisition system: bulk and three heater temperatures and the pressure inside the vessel. When the finned tubes are used then firstly they had to be mounted over the heater rod. Accordingly four other thermocouples located in the finned tube are also recorded.

Externally finned tubes that are used in industry vary in fin density, height and structure. For boiling applications only low finned tubes, varying in fin height between approximately 0.4 and 1.5 mm and in fin density between approximately 16 and 43 fpi, are utilized. This is due to the lower fin efficiency which is expected for medium- and high-finned tubes (Thome, 1990). The fin efficiency decreases with increasing fin height due to the decrease in fin temperature with length (Bejan and Kraus, 2003). The dimensions of the investigated tubes, including plain and low-finned stainless steel tubes are given in Table 1.

Table.1: Dimensions of test tubes

	Type	Material	Fin density [fpi]	Fin height [mm]	d_i [mm]	d_o [mm]
	Plain	316 Stainless steel	-	0	10.68	14.94
	Finned	Stainless steel	19	1.5	12.50	18.60
	Finned	316 Stainless steel	40	0.8	15.06	18.97
	High-performance finned	316 Stainless steel	40	0.7	15.10	18.92

The roughness R_a of the plain stainless steel tube was kept approximately at a value of 0.6 µm. The fin density of the finned tubes is 19 and 40 fpi with a fin height of 1.5 and 0.8 mm, respectively. The fins of the high performance finned tubes (40 fpi, 0.7 mm fin height) are compressed at regular intervals to a second fin height level. Since the inner diameter of the investigated tubes is larger than the outer diameter of the heater rod, a fixing tube which fills the gap was necessary. The fixing tube is made out of copper and is pressed into the finned tube. The assembly of the tubes is shown in Fig. 3.

The finned tube together with the fixing tube is pulled on the HTRI heater rod. For reducing the thermal contact resistance between the fixing tube and the heater rod, a thermally conductive paste “Akasa Silver Compound 450” is used to fill the gap. The thermal conductivity of the paste is 9.24 W/m·K. For the calculation of surface temperature of the finned tubes, four thermocouples (type K, diameter 0.5 mm) were embedded in the wall of the finned tube which were arranged in 90° with respect to each other as shown in Fig. 3. The thermocouples and the test tubes are fixed at the edge on the heater rod with high temperature resistant silicon.

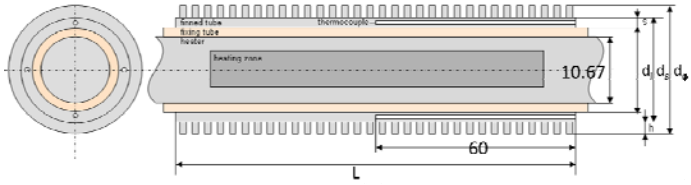

Fig. 3 Assembly of investigated finned tubes (all dimensions in mm and other parameters defined in Table 1).

2.3 Test Solution

Experiments were conducted using saturated $CaSO_4$ solutions with inverse solubility with respect to temperature. During boiling at ambient pressure the concentration of a saturated calcium sulphate solution is 1.6 g/L. In the present study $CaSO_4 \cdot ½\ H_2O$ was dissolved at ambient temperature in distilled water. Calcium sulphate hemihydrate which was used in this study has a purity of 97%. The weight of powder for preparing a saturated solution at the boiling point under ambient pressure, i.e. 1.6 g/L, is calculated according to:

$$m_{CaSO_4 \cdot ½ H_2O} = c_{CaSO_4} \cdot V_{H_2O} \cdot \left(\frac{M_{CaSO_4 \cdot ½ H_2O}}{M_{CaSO_4}} \right) \cdot \left(\frac{100}{purity} \right) \quad (1)$$

For preparing 30 litres of saturated $CaSO_4$ solution, the required amount of $CaSO_4 \cdot ½\ H_2O$ powder is calculated to be 60 g. Since calcium sulphate can hardly be dissolved in water, the solution is mixed for about 8 hours with a stirrer and left over night before entering it into the test rig to allow any possible sediment to settle down. During these 24 hours preparation time, the solution is held in open container thus local evaporation may occur. Therefore the amount of $CaSO_4 \cdot ½\ H_2O$ powder for preparing a 1.6 g/L $CaSO_4$ solution was experienced to be 55 g. The concentration of the test solution is measured by titration using complexometric ethylenediaminetetraacetic acid (EDTA) before starting each experiment.

2.4 Test Run Procedure

After the preparation of the test solution and once the test tube is mounted then the solution is introduced into the vessel up to 3 cm below the top of the vessel by generating a vacuum with the vacuum pump. Vacuum is also used for degassing the solution. Turning on the cooling flow gives a natural siphon for degassing. During preheating of the test solution with the vessel band heater, the vacuum drops naturally, as the solution vapour pressure increases. Starting the data acquisition system allows control of the temperature inside the vessel. After approximately 3 hours of preheating, the test solution reaches saturation temperature. In the case of calcium sulphate solution as working solution, a sample is taken out of the vessel for concentration analysis. Depending on the conducted experiment, the recording interval of the data acquisition system is selected to be 30 s.

After steady state is reached at saturation temperature, the heater is then turned on applying the desired heat flux. In the following 20 min the cooling water flow needs to be adjusted manually for ensuring saturation temperature in the bulk. During the experiment videos are also recorded by the high speed camera. After certain time elapsed the thermal shock is applied i.e. sudden turning-off of the heat flux transferred and turning-on again after approximately 30 s. At the end of each fouling experiment the heat flux is reduced gradually until it is turned off to maintain the fouling layer unscathed on the test tube. After draining the water and removing the heater with the test tube, pictures are taken of the test tube for documentation of the fouling layer structure. Before starting the next fouling run, the vessel has to be cleaned by removing the front view port glass and cleaning the vessel wall with water. Tenacious scale on the roof of the vessel is removed by a spoon.

2.5 Data Reduction

A computer controlled data acquisition system was used to measure the pressure inside the vessel, the bulk temperature and the temperatures of the thermocouples located in the test tube and the heater rod. All fouling experiments are conducted at constant heat flux. The heat flux is calculated out of the measured heater voltage and current and where "A" is the heat transfer area:

$$\dot{q} = \frac{V \cdot I}{A} \quad (2)$$

For structured tubes the calculation of the area "A" is based on the outer diameter of the tubes.

$$A = \pi \cdot d_o \cdot L_{heating\ zone} \quad (3)$$

The heat transfer coefficient and the fouling resistance can be calculated according to:

$$\alpha = \frac{\dot{q}}{(T_s - T_b)} \quad (4)$$

$$R_f = \left(\frac{T_s - T_b}{\dot{q}} \right)_t - \left(\frac{T_s - T_b}{\dot{q}} \right)_{t=0} \quad (5)$$

The average surface temperature of the test tubes is calculated according to arithmetic average of the four thermocouples arranged in the test tube as shown in Fig. 4.

$$T_s = T_{TC} - \frac{d_s \cdot \dot{q}}{2 \cdot \lambda} \ln\left(\frac{d_s}{d_{TC}} \right) \quad (6)$$

As the distance of the thermocouples to the surface considerably is smaller than the diameter of the heater rod ($s << d$), the formulas for heat conduction in flat plates can be applied.

$$T_s = T_{TC} - \frac{\dot{q}}{\lambda / s} \quad (7)$$

Since the HTRI heater consists of different layers of various materials with the lack of information concerning the thickness and thermal conductivity of theses layers, the surface temperature of the heater needs to be calculated using an empirical constant λ/s. After the determination of the heat transfer coefficient with the Gorenflo correlation (1993), the surface temperature of the heater rod can be calculated and the constant λ/s determined as 12,500 W/m²K.

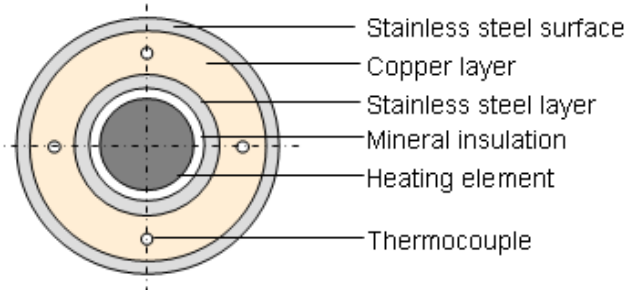

Fig. 4 Cross section of heater rod.

3 RESULTS AND DISCUSSION

3.1 Fouling of plain and finned tubes

Esawy (2011) and Thome (1990) showed the enhanced heat transfer performance of structured tubes is due to lower superheat on an enhanced boiling surface to that of the plain surface. As scale formation during boiling of calcium sulphate is caused by supersaturation on the heat transfer surface (Jamialahmadi and Müller-Steinhagen, 1993), thus lower fouling should occur on structured surfaces than on plain surfaces.

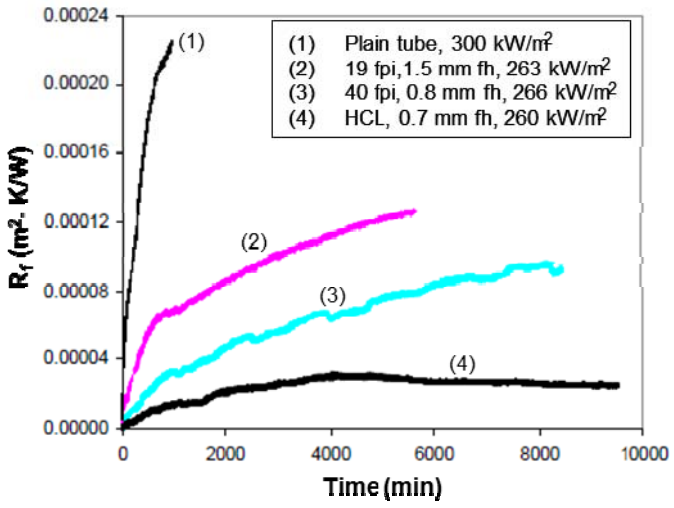

Fig. 5 Fouling behaviour of plain, 19, 40 fpi and HCL tube with time during boiling of 1.6 g/L $CaSO_4$ at 260 to 300 kW/m².

Fig. 5 compares fouling characteristics of various structured tubes for heat fluxes ranging from 260 to 300 kW/m² to that of the plain tube. If one neglects the variation of heat flux, then the finned tubes show overall significantly reduced fouling resistance with time to that of the plain tube. The HCL tube undoubtedly shows the best performance, because after 1000 min, the fouling resistance was only 7% of the plain tube. All investigated finned tubes tend to show asymptotic behaviour in fouling resistance after a certain operating time. With increasing fin density less fouling occurs on the heat transfer surface.

Fig. 6 presents several typical pictures which were recorded during boiling of 1.6 g/L $CaSO_4$ at 263 kW/m² with the 19 fpi tube as time elapses. The pictures show distinct behaviour to that of a plain tube in particular much lower deposition (Esawy et al, 2009). They attributed this to i) lower surface temperature of fins compared to that of the plain tube; ii) wiping action of bubbles and iii) the fins would act as cutting edge that prevent the binding of crystals to form a homogenous deposit layer.

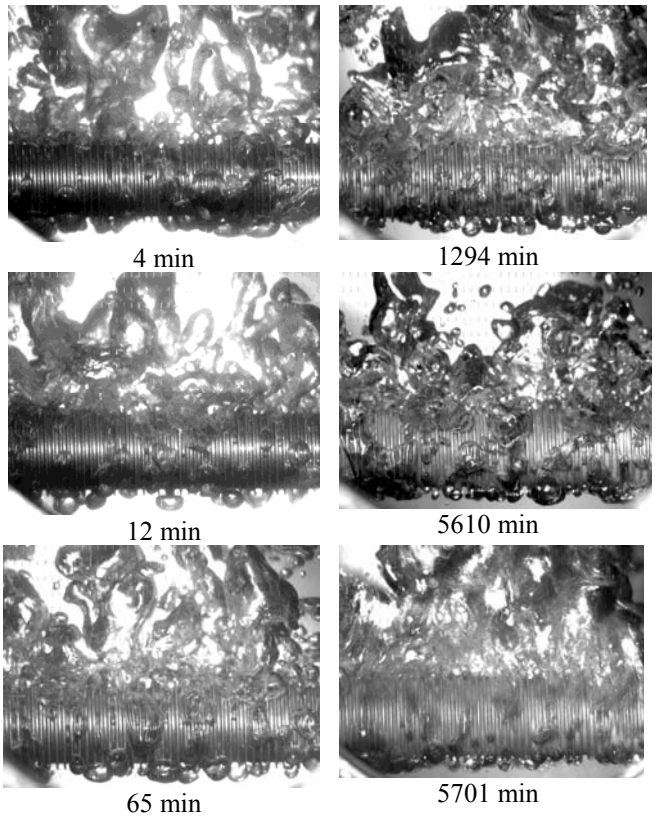

Fig. 6 Bubble behaviour on 19 fpi tube during boiling of 1.6 g/L $CaSO_4$ at 263 kW/m².

In addition, pictures of the deposit layer on the structured tubes are presented in Fig. 7 which were taken at the end of fouling run. Esawy et al. (2009) reported that on the plain tubes the deposit layer is a homogeneous thick layer of $CaSO_4$. On the finned tubes, nonetheless, as shown in this figure, the scale precipitates primarily only on the base surface. As the largest temperature exists on the base of finned tubes (Esawy, 2011) and bubbles are preferably generated there, thus supersaturation and scale formation occurs primarily on the base surface area. Furthermore, agitation of the rising bubbles in the fin channels

counteracts the formation of deposits on the flank of the fins. Only at some scattered small spots on the 40 fpi tube, the fins are completely covered with scale. Reasons for these spots may be related to the lower fin height of the 40 fpi tube.

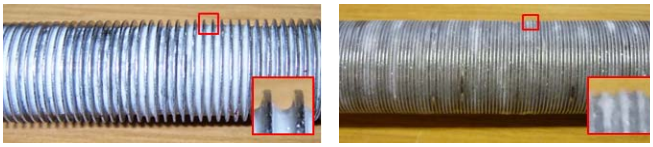

19 fpi tube after 3176 min at 266 kW/m²

40 fpi tube after 8475 min at 266 kW/m²

Fig. 7 Fouling layer on structured tubes during boiling of 1.6 g/L $CaSO_4$ solutions.

3.3 Impact of thermal shock on smooth tubes

Short-time under- or overheating of the heat transfer surfaces may cause brittle deposit layers to crack due to the different thermal expansion of tubes and deposits. The applicability of thermal shocks for cleaning purposes is tested during fouling experiments, i.e. sudden switching-off of the heat flux followed by switching-on again after approximately 30 s.

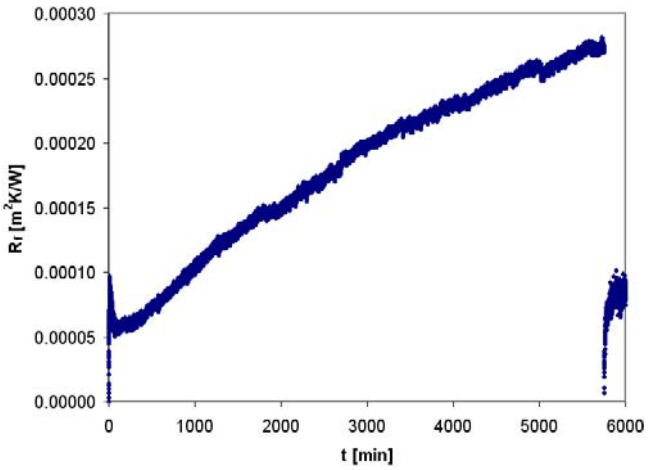

Fig. 8 Thermal shock on the bare heater during boiling of 1.6 g/L $CaSO_4$ solution at 80 kW/m².

Figs. 8 and 9 demonstrate the impact of thermal shock on cleaning of the plain tube for heat fluxes of 80 and 300 kW/m². Fig. 9, in particular, shows multiple thermal shocks at different time intervals. The results presented in these figures generally show that:

- the thermal shock can effectively clean the surface of the plain tube;
- the fouling resistance after thermal shock starts close to zero which implicates a somewhat total removal of the fouling layer from the heat transfer surface;
- the behaviour of fouling curve differs in the initial period after the thermal shock with that of a clean surface which has been used only once. The initial period on the latter it consisted of rapid increase in fouling resistance due to fast growth of deposit layer followed by a decrease due to increased number of bubbles which resulted from higher number of nucleation sites before reaching a plateau. Once thermal shock is applied however, the surface showed only increase in fouling resistance in linear manner. The presence of scattered and small number of remaining small crystals that are supposedly left on the surface should be accounted for this behaviour;
- and finally at 300 kW/m^2 when repeated thermal shocks are applied then the surface starts from near zero even though the gap between two shocks are short;

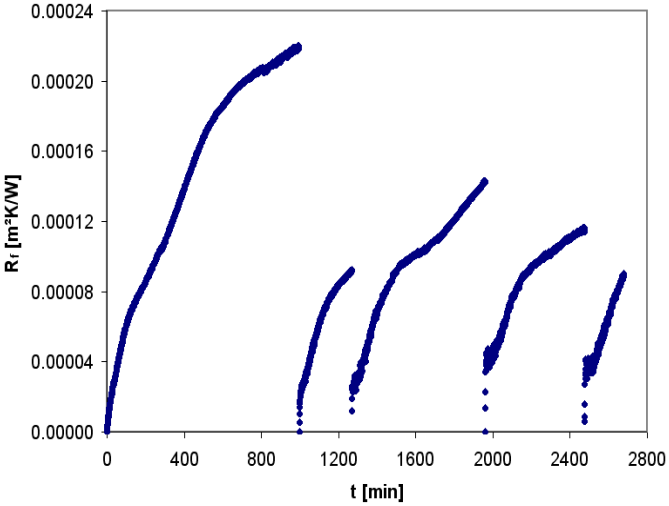

Fig. 9 Thermal shock on the plain surface during boiling of 1.6 g/l $CaSO_4$ solution at 300 kW/m².

It should be pointed out that the initial increase in fouling resistance near time zero in Fig. 8 actually occurs over a significant time. The apparently sharp increase is due to the long time span of X-axis. Malayeri and Müller-Steinhagen (2007) showed that for the first few minutes, the fouling resistance increases gradually before reaches a plateau followed by yet another reduction then finally increases again. This has also been shown before by other researchers (Palen and Westwater, 1966; Jamialahmadi and Müller-Steinhagen, 1993). At time 5800 min though, the sharp increase of fouling resistance is genuine as the remaining small crystals, assuming the cleaning is not 100%, would serve as nucleation site that cause rapid crystallization which in turn cause fouling resistance to increase sharply.

Video recording of the thermal shocks provides also information about the effectiveness of cleaning. For heat fluxes of 80 and 200 kW/m², the fouling layer cracks then is peeled off by the bubble agitation after the sudden increase in heat flux but are not shown here for the sake of brevity. For the heat flux 300 kW/m², nevertheless, the crack and peeling off of the deposit layer occurred when the heat flux is suddenly switched-off for 30 s as shown in Fig. 10. As it

can also be seen, the deposit is taken off from the surface in relatively large pieces.

Having examined these results one can assume that cracking is caused due to thermal expansion/contraction of the surface. During contraction of the surface, the fouling layer is detached from the heat transfer surface. Cracking either occurred during detachment or after detachment by the bubble agitation. The coefficient of thermal expansion of stainless steel is 17×10^{-6} K^{-1} (Ho and Taylor, 1998), and for calcium sulphate 22×10^{-6} K^{-1} (Goyal, 2004). Due to the low thickness of the fouling layer, its expansion/contraction can be neglected. The length of thermal expansion/contraction of the surface can be calculated with following equation:

$$\Delta l = \alpha_l \cdot \Delta T \cdot l_o \qquad (8)$$

Assuming a surface temperature of 140°C (ΔT≈40 K) the thermal expansion/contraction of the heater rod diameter 10.68 mm is 7 µm.

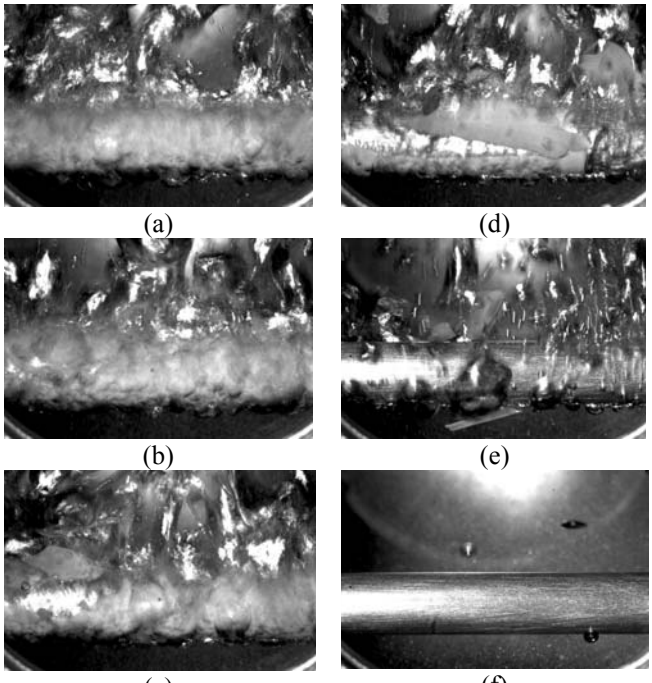

Fig. 10 Thermal shock on the plain surface after 105 min boiling of 1.6 g/L $CaSO_4$ solution at 300 kW/m² (a-f represent time sequence at every 0.05 sec).

3.4 Impact of thermal shock on finned tubes

Thermal shock experiments, i.e. sudden reduction in heat flux for approximately 30 s during fouling experiments, are also conducted for the 19, 27 and 40 fpi tubes after 5640, 5122 and 8463 min boiling of 1.6 g/L $CaSO_4$ at 263, 300 and 266 kW/m², respectively. Contrariwise to the promising results which were obtained for the plain tube as shown previously, the results on the finned tubes show that the fouling layer is only marginally affected by the applied thermal shock. Experimental results and several pictures recorded during the thermal shock on the 19 fpi tube are presented in Figs. 11 and 12.

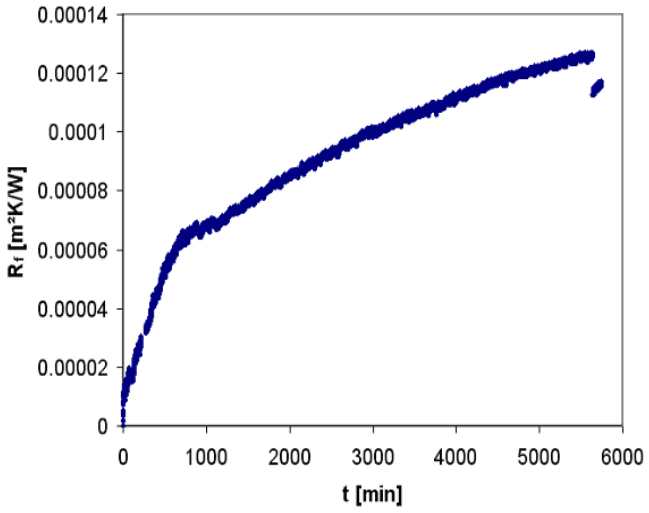

Fig. 11 Thermal shock on 19 fpi tube during boiling of 1.6 g/L $CaSO_4$ at 263 kW/m².

The thermal shock is applied after 5640 min but the fouling resistance is just marginally reduced. The sequence of pictures in Fig. 12 does not show any noticeable removal of the deposit during the sudden reduction in heat flux. In addition, the bubble behaviour does not differ before and after the thermal shock.

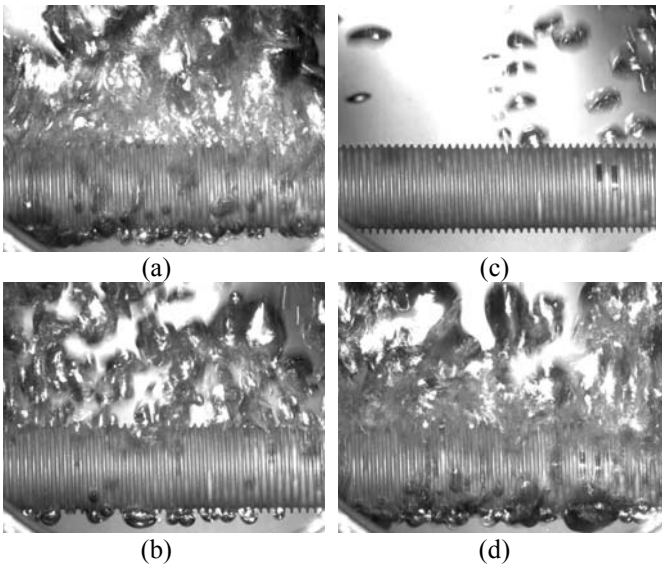

Fig. 12 Thermal shock on 19 fpi tube after 5640 min boiling of 1.6 g/L $CaSO_4$ at 263 kW/m² (a-d represent time sequence at every 0.05 sec).

4. CONCLUSIONS

Experiments were performed on the plain and numerous finned tubes to characterize the impact of thermal shock on cleaning the surface during crystallization fouling of $CaSO_4$ at boiling conditions. The best cleaning performance was obtained on the plain tube for all investigated heat fluxes in this study. Two important

features of thermal contraction/expansion as well as continuing turbulence caused by movement of bubbles are responsible for this behaviour. On the contrary for the finned tubes, the experimental results implicated only minor improvement in heat transfer when thermal shock is applied.

NOMENCLATURE

A	area of the heat transferring surface, m^2
A_b	base surface area, m^2
C_b	bulk concentration, g/L
d_b	base diameter, m
d_i	finned tube inner diameter, m
d_o	finned tube outer diameter, m
d_s	surface diameter, mm
d_{th}	diameter of thermocouple location, m
h	fin height, mm
I	measured electric current
k	thermal conductivity, W/m·K
L	heater heating zone length, mm
l_0	initial length before expansion/contraction, m
m	fin pitch, mm
MW	molecular weight, g/mol
$\dot{q}$	heat flux, W/m^2
q	rate of heat transfer, W
R_f	fouling resistance, $m^2 \cdot K/W$
s	distance between the thermocouple and surface, mm
T_b	bulk temperature, K
T_s	surface temperature, K
T_{TC}	temperature of thermocouple, K
t	time, s
V	heater voltage, V
W	weight, g

Greek symbols

α	heat transfer coefficient, $W/m^2 \cdot K$
α_l	coefficient of thermal expansion, K^{-1}
λ	thermal conductivity, W/K·m

Abbreviations

fh	fin height
fpi	fin per inch

ACKNOWLEDGMENTS

The finned tubes were supplied by Wieland GmbH, Germany, MPG GmbH, Germany for which the authors are grateful.

REFERENCES

Behbahani, R.M., Jamialahmadi, M., Müller-Steinhagen, H., 2005, Pool boiling heat transfer to phosphoric acid solutions, *Heat Transfer Eng.*, Vol.26, No.4, pp.26-34.

Bejan, A., Kraus, A.D., 2003, Heat transfer handbook, Wiley.

Esawy, M., 2011, Fouling of structured surfaces during pool boiling of aqueous solutions, *PhD thesis*, University of Stuttgart.

Esawy, M., Malayeri, M.R. and Müller-Steinhagen, H., 2010, Crystallization fouling of finned tubes during pool boiling: Effect of fin density, *J. Heat and Mass Transfer*, Vol. 46, pp. 1167-1176.

Gorenflo, D., 1993, Pool boiling. In VDI Gesellschaft Verfahrenstechnik und Chemieingenieurwesen, *English translation of VDI*, Düsseldorf, Ha 4-Ha 18.

Gourdon, M., Vamling, L., Andersson, U., Olausson, L., 2010, Crystallization in a pilot evaporator: Aqueous solutions of Na_2CO_3 and Na_2SO_4, *Industrial & Engineering Chemistry Research*, Vol. 49, No.5, pp.2401-2409.

Goyal, M., Biomaterials for othopaedics, *University of Puerto Rico, viewed* 24.09.2010: http://academic.uprm.edu/~mgoyal/materialsmay2004/k04orthopaedicppt.pdf

Ho, C.Y., Taylor, R.E., 1998, Thermal expansion of solids, CINDAS Data series on material properties, Vol.1-4, *ASM International*.

Hospeti, N.B., Mesler, R.B., 1965, Deposits formed beneath bubbles during nucleate boiling of radioactive calcium sulphate solutions, *AIChE Journal*, Vol.11, No.4, pp. 662-665.

Jamialahmadi, M., and Müller-Steinhagen, H., 1993, Scale formation during nucleate boiling- a review, *Corrosion Reviews*, Vol.11, No.1&2, pp. 25-54.

Malayeri, M.R., and Müller-Steinhagen, H., 2007, Initiation of $CaSO_4$ scale formation on heat transfer surfaces under pool boiling conditions, *Heat Transfer Eng.*, Vol. 28, No. 3, pp. 240-247.

Müller-Steinhagen, H., Malayeri, M.R. and Watkinson, A.P., 2011, Heat exchanger fouling: Cleaning and mitigation techniques, *Heat Transfer Eng.*, Vol. 32, Nos. 3-4, pp. 189-196.

Palen, J.W., and Westwater, J.W., 1966, Heat Transfer and Fouling Rates during Pool Boiling of Calcium Sulphate Solutions, *Chem. Eng. Prog. Symp. Series*, Vol. 62, No. 64, pp. 77–86.

Schwarz, T., 2001, Heat transfer and fouling behaviour of Siemens PWR steam generators- long-term operating experience, *Experimental Thermal and Fluid Science*, Vol.25, No.5, pp.319-327.

Thome, J.R., 1990, *Enhanced boiling heat transfer*, Chapter 4, p. 64, Hemisphere Publishing Corporation.